Energy-Efficient Resource Allocation in Multi-UAV Networks With NOMA

Saif Najmeddin, *Graduate Student Member, IEEE*, Sonia Aïssa, *Fellow, IEEE*, and Sofiène Tahar, *Senior Member, IEEE*

***Abstract*—This paper investigates the energy efficiency (EE) optimization in a wireless communication network where multiple UAVs serve different types of devices, namely, information receivers (IRs) and energy receivers (ERs). The UAVs transmit power signals towards the ERs, and then enable data transmission to IRs on the downlink and from ERs on the uplink with non-orthogonal multiple access (NOMA). The optimization problem to maximize the overall EE is formulated and solved using Lagrangian optimization and gradient-descent methods. The optimization is decomposed into two sub-problems. Firstly, by connecting the path loss of the devices' channels with their rate demands, the UAVs' optimal positions are obtained. Then, based on the obtained UAVs' optimal positions and a closed-form expression for the EE, a resource allocation aiming to maximize EE is developed. For the simulations, two main scenarios for single and multiple UAVs are considered. Numerical results and comparisons are provided. In particular, for the single-UAV scenario, the results show an enhancement in EE for the operation with NOMA compared with OMA. For the multiple-UAV scenario, several cases depending on different combinations of the devices' rate requirements are considered. The results show the superiority of NOMA over OMA in all use cases. The results also reveal the effect of considering the devices' rate requirements on the EE, where the case with equal rate requirements has the best performance.**

***Index Terms*—UAV, wireless power transfer, WIPT, NOMA, resource allocation, energy efficiency.**

I. Introduction

UNMANNED aerial vehicles (UAVs) are becoming more reachable and available to be used in numerous applications. With their cost-effectiveness, flexibility, and 3D mobility, UAVs are considered to be an appealing and efficient solution for many challenges. One of UAVs' crucial applications is in the area of wireless communications, where reliable and cost-effective services can be provided through a network of single or multiple UAVs [1]. For example, UAVs can be deployed to enable power and information transfer in Internet of things (IoT) networks, in which the devices are energy-constrained and their limited battery capacity may not allow communication over long ranges [2], [3]. Depending on the application, an UAV can enable service to/from different types of devices, namely, devices transmitting and/or receiving data, termed information receivers (IR) hereafter, and devices capable of harvesting energy and transmitting data, referred to as energy receivers (ER) hereafter. In fact, UAVs can be efficiently used to charge ERs via downlink wireless power transfer (WPT) to enable their data communication on the uplink, and also transmit data to IRs according to their service requirements.

In many B5G use cases, its expected that UAVs will be called to concurrently serve ERs and IRs to provide efficient WPT along with reliable data services. The use of such a concept needs to meet the radio resource sharing of B5G, where non-orthogonal multiple access (NOMA) will very likely be replacing the conventional orthogonal multiple access (OMA) approach [4]. In fact, NOMA has recently received significant attention for its promising performance. However, this comes with additional complexity, where successive interference cancellation (SIC) has to be performed for reliable services [5], [6].

Although the use of UAV to serve multiple IRs and ERs based on the NOMA scheme is interesting and promising, this comes with many challenges, including the limited power budget of the UAV, the constraints on its positioning, the devices' quality of service (QoS) requirements, etc. Intuitively, additional complexities appear when the network involves multiple UAVs, which is becoming essential in many use cases to enhance the coverage of the network. For example, a collision avoidance scheme should be in place. Moreover, unlike single-UAV networks, where all devices are linked to the same UAV, the device association problem in deployment cases with multiple UAVs has to be tackled efficiently.

A. Related Work

In the related literature, some works focused on the resource allocation to enhance the performance of UAV-enabled WPT or wireless information transfer. For instance, the work in [7] addressed maximization of the system throughput by exploiting trajectory design of the UAV jointly with the resource allocation optimization, where a single UAV transfers power to multiple ERs by changing its position periodically. The authors

Manuscript received February 15, 2021; revised May 20, 2021 and July 19, 2021; accepted July 20, 2021. Date of publication July 30, 2021; date of current version November 22, 2021. This article was presented in part at the 2020 IEEE Global Communication Conference, Taipei, Taiwan. *(Corresponding author: Saif Najmeddin.)*

Saif Najmeddin is with the ECE Department, Concordia University, Montreal, QC H3G 1M8, Canada, and also with the Institut National de la Recherche Scientifique, Montreal, QC H5A 1K6, Canada (e-mail: s_najmed@ece.concordia.ca).

Sonia Aïssa is with the Institut National de la Recherche Scientifique, Montreal, QC H5A 1K6, Canada (e-mail: sonia.aissa@inrs.ca).

Sofiène Tahar is with the ECE Department, Concordia University, Montreal, QC H3G 1M8, Canada (e-mail: tahar@ece.concordia.ca).

Digital Object Identifier 10.1109/TGCN.2021.3101200

in [8] investigated the energy efficiency optimization in a WPT network, where ERs are wirelessly powered from a single UAV to enable their uplink information transmission, by optimizing the transmit power towards each ER after getting the optimal placement of the UAV. In [9], a placement algorithm was proposed to optimize the UAV transmit power and maximize the coverage of the ground nodes (GNs). Also, the authors of [10] considered the perfect user location information (ULI) to maximize the system throughput by optimizing the UAV placement. In [11], on the other hand, partial ULI was used to develop an adaptive UAV deployment scheme, where the position of the UAV is optimized based on limited information about the GNs.

Few other works considered networks where several IRs and ERs are served by a single UAV. The work in [12] studied the problem of maximizing the end-to-end cooperative throughput for a network of UAV-enabled simultaneous wireless information and power transfer (SWIPT), by optimizing the UAV's decision profile, power profile, and trajectory, for different protocols. Also, [13] considered a SWIPT network that consists of a single UAV and IoT devices, and applied concave-convex procedure to maximize the devices' minimum rates. In [14], the authors considered a network of IoT devices enabled by a single UAV, and tackled maximization of the minimum harvested energy among the IoT devices by optimizing the power allocation and the trajectory design of the UAV. Leveraging the benefits of NOMA over OMA, the work in [15] proposed a cooperative NOMA scheme to maximize the weighted sum-rate of the UAV and GNs by optimizing the power allocations and the UAV's rate. Furthermore, minimization of the energy consumption of GNs with acceptable QoS was tackled in [16], where offloading was enabled by uplink and downlink communications between the GNs and the UAV via NOMA or OMA protocols.

In addition to the above, few studies investigated the performance of multiple-UAV communication systems. For instance, the authors of [17] investigated the download coverage probability in a network of multiple UAVs which were modeled as a uniform binomial point process at the same altitude. The work in [18] investigated stochastic modelling of UAV base stations, where different coverage models were suggested. Also, [19] studied the maximization of the minimum data rate of GNs by jointly optimizing the 3D locations, user association, and power allocation in multiple-UAV networks.

The aforementioned works have presented promising results in this area, but there is considerable potential for further gains. For example, many works considered single-antenna UAV in the models, which basically degrades the UAV's ability to meet the service requirements of the GNs. Also, only a few works considered scenarios with multiple UAVs, which are crucial to provide efficient coverage in most practical cases. Furthermore, some systems were based on the OMA scheme, with no consideration of NOMA. Moreover, most works ignored the most critical aspect in this particular setup, namely, energy efficiency (EE), which is extremely important as we are dealing with limited on-board energy resources. Due to its significant impact on performance, EE of UAV-aided communication systems requires careful consideration.

B. Contributions

In this work, we address the optimization of the EE of a wireless network, where several multiple-antenna UAVs serve as simultaneous power and information transmitters towards ERs and IRs, respectively, and where energy harvested by the ERs is used for their uplink communications towards their associated UAV, based on NOMA scheme. Considering partial ULI about the ERs and IRs, we present a user distribution and association model for each device cluster in the network. We propose collision avoidance constraints to avoid UAVs' collisions as they move to enhance the links for the ERs and IRs. Moreover, a time allocation scheme is enabled to specify the optimal switching between the energy and information transmissions. We also consider several constraints on the main system parameters, including the required QoS of the devices, and the thresholds to enable SIC. Considering the aforementioned constraints, we propose two algorithms to maximize the EE by first optimizing the UAVs' positions and then optimizing the power pertaining to the IR and ER devices in each cluster.

Specifically, the main contributions of this paper can be summarized as follows: **(i)** We present a system model of multiple-UAV enabled WIPT with NOMA. We formulate and solve a highly coupled non-convex optimization problem, where the goal is to maximize the system's EE while satisfying constraints related to user association, power budget, collision avoidance, acceptable QoS, and SIC thresholds. **(ii)** We propose two algorithms to solve the EE maximization problem based on the Lagrangian multipliers and gradient-descent method. Firstly, we optimize the UAVs' locations to provide better transmission links for the ERs and IRs; this is done by introducing a demand requirement variable and connecting it to the path loss of each device. Secondly, we optimize the power for each ER and IR to maximize the EE. **(iii)** We conduct extensive simulations to assess the effectiveness of the proposed algorithms in two scenarios. For the single-UAV scenario, we detail the superiority of the NOMA-based scheme over the OMA scheme. For the multiple-UAV scenario, we present different cases based on different combinations of the devices' QoS requirements, and provide a comparison between all cases for the NOMA and OMA schemes.

Next, Section II details the network model. Formulation of the EE is described in Section III-A. The optimization problem is formulated and solved in Section III. Numerical results are presented and discussed in Section IV. Finally, Section V concludes the paper.[1]

II. System and Channel Models

A. Multiple-UAV Based WIPT

A network of multiple devices that are enabled by multiple UAVs is considered. There are two types of devices; IRs and ERs. We consider M multi-antenna UAVs serving several single-antenna devices that are distributed in a region of interest (ROI) (Fig. 1). We assume that the ROI can be divided

[1] *Notation:* Symbol $\mathbb{E}\{.\}$ is used for the expectation operator, $(.)^{\dagger}$ denotes the conjugate transpose, $|.|$ denotes the modulus, $\|.\|$ is the Euclidian norm, and $[.]^{+}$ refers to $\max(0,.)$.

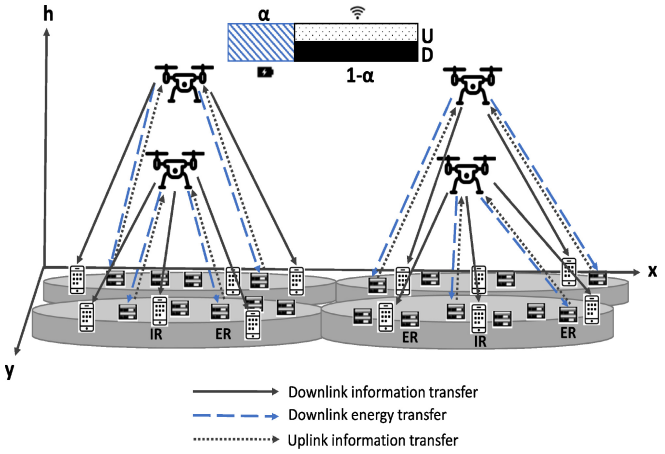

Fig. 1. Multiple-UAV wireless information and power transfer network.

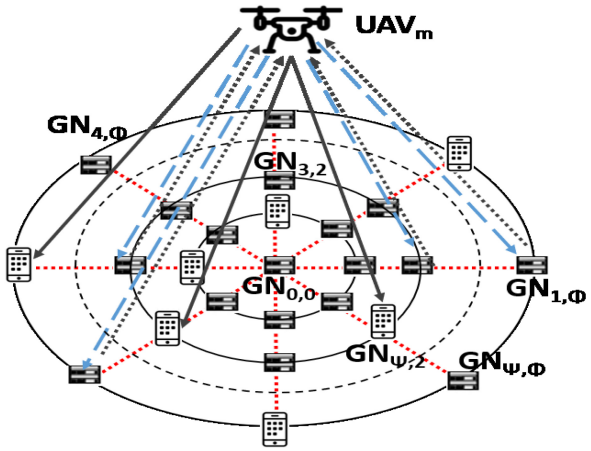

Fig. 2. Distribution of devices in cluster m.

into a number of clusters that can be determined to provide the required coverage for the ROI, such that each cluster of devices will be served by a single UAV. A UAV does not have perfect ULI of the devices in its cluster. The total number of antennas at the UAV is $N = N_{\mathrm{E}} + N_{\mathrm{I}}$, with N_{E} used for the ERs, and N_{I} dedicated to the IRs; this is the same for all UAVs. The time slot T is divided into two phases. In the first phase, $\alpha_m T$ $(0 < \alpha_m < 1)$, each UAV transmits energy signals to the scheduled ERs in its cluster. In the second phase, $(1-\alpha_m)T$, the ERs make use of the harvested energy to transmit their always-available data to their associated UAV, while the UAV transmits information to the IRs, simultaneously. The data transmissions on the uplink (U) and downlink (D) are performed according to the NOMA protocol. Without loss of generality, the time slot duration T is set to unity. The position of UAV_m, $m = 1, \ldots, M$, is denoted by (x_m, y_m, h_m).

B. Distribution of Devices

We consider the partial ULI approach [20]. Initially, a UAV will not have perfect information about the locations of the GNs. Each UAV will be sent to a specific cluster in the ROI. A cluster is defined as a circular coverage area of radius r_m. The partial information that is known by a given UAV is the distribution of the GNs within its cluster [21]. Specifically, we consider that a cluster is subdivided into rings and segments as shown in Fig. 2. Denote the number of rings as Φ and the number of segments as Ψ. The rings are co-centered around the origin and are such that the radius of the outer circle of ring ϕ is $r_m\phi/\Phi$, and the angle between any two adjacent segments is $2\pi/\Psi$. At the beginning, each UAV will be hovering at the minimum allowable height over the center of its corresponding cluster, then the devices that need to be served will send side information to the UAV with the best link to each of them, which usually has the shortest distance to each of them. This information is related to their identities, e.g., ID of the GN located on the intersection between segment ψ and circle ϕ is (ψ, ϕ) (cf. Fig. 2), along with their rate demands. Based on the received information and the predetermined number of scheduled GNs, the UAV chooses the devices that will be served within its cluster, and positions itself accordingly to start sending power and sending/receiving data.

For simplicity of exposition, we replace the notation $\mathrm{GN}_{\psi,\phi}$ depending on the device type. The notation becomes $\mathrm{ER}_{m,j}$ for ER devices, $\mathrm{IR}_{m,k}$ for the IR nodes. In each cluster, there are J ERs and K IRs. The location of $\mathrm{ER}_{m,j}$ is denoted $(x_{\mathrm{ER}_j}, y_{\mathrm{ER}_j}, h_{\mathrm{ER}_j})$, and the one of $\mathrm{IR}_{m,k}$ is denoted $(x_{\mathrm{IR}_k}, y_{\mathrm{IR}_k}, h_{\mathrm{IR}_k})$. A quantized level of the uplink rate requirement is sent from each ER to its associated UAV to indicate its WPT demand. Based on this side information, and knowledge of the rate requirements of the IRs, each UAV determines the relative demand of each ER and IR, denoted Υ_j^{U} and Υ_k^{D}, respectively, such that $\sum_{j,k} \Upsilon_j^{\mathrm{U}} + \Upsilon_k^{\mathrm{D}} = 1$. Here, a larger value of Υ means a higher rate demand. A binary variable of ER association with a specific UAV_m is denoted $\chi_{m,j}$, and the one for IR is denoted $\chi_{m,k}$. If $\mathrm{ER}_{m,j}$ is served by UAV_m, then $\chi_{m,j} = 1$, otherwise it is zero. Note that UAV_m can serve multiple ERs and IRs; but each device can only be served by one UAV. These can be formulated as follows:

$$\sum_{m=1}^{M} \chi_{m,j} = 1, \quad \forall j. \tag{1}$$

$$\sum_{m=1}^{M} \chi_{m,k} = 1, \quad \forall k. \tag{2}$$

$$\chi_{m,j} \in \{0,1\}, \quad \forall m, \forall j. \tag{3}$$

$$\chi_{m,k} \in \{0,1\}, \quad \forall m, \forall k. \tag{4}$$

C. Channel Models

There are three types of channels in the network: 1) air-to-ground (A2G) from the UAVs to IRs and ERs; 2) ground-to-air (G2A) from the ERs to the UAVs; and 3) ground-to-ground (G2G) between the ERs and IRs. Consider UAV_m, $m = 1, \ldots, M$. The complex channel vector of the A2G link UAV_m-$\mathrm{ER}_{m,j}$ is denoted $\mathbf{g}_{m,j} \in \mathbb{C}^{1\times N_{\mathrm{E}}}$, for $j = 1, \ldots, J$. For the A2G link UAV_m-$\mathrm{IR}_{m,k}$, $k = 1, \ldots, K$, the complex channel vector of the A2G link is denoted $\mathbf{h}_{m,k} \in \mathbb{C}^{1\times N_{\mathrm{I}}}$. First, we have N_{I}. First, we have $\mathbf{g}_{m,j} = \mathbf{g}'_{m,j}/\sqrt{L^{\mathrm{D}}_{\mathrm{ER}_{m,j}}}$, where $L^{\mathrm{D}}_{\mathrm{ER}_{m,j}}$ is the average path-loss, and

$\mathbf{g}'_{m,j} = [g'_{m,j_1}, g'_{m,j_2}, \ldots, g'_{m,j_{N_\mathrm{E}}}]$ is the normalized channel fading vector. With Rician fading, $\mathbf{g}'_{m,j}$ can be written as [8]:

$$\mathbf{g}'_{\mathbf{m,j}} = \sqrt{\frac{\mathcal{K}}{\mathcal{K}+1}}\mathbf{1}_{1\times N_E} + \sqrt{\frac{1}{\mathcal{K}+1}}\tilde{\mathbf{g}}_{m,j}, \tag{5}$$

where $\mathcal{K}$ is the Rice factor, $\mathbf{1}_{1\times N_E}$ is a unity row vector, and the non-line-of-sight (NLoS) fading component $\tilde{\mathbf{g}}_{m,j}$ is a row vector the elements of which are i.i.d. complex Gaussian random variables with zero mean and unit variance, i.e., $\mathcal{CN}(0,1)$. The average A2G free-space distance-dependent path loss of $\mathrm{ER}_{m,j}$, $L^{\mathrm{D}}_{\mathrm{ER}_{m,j}}$ in dB, is given by:

$$L^{\mathrm{D}}_{\mathrm{ER}_{m,j}} = p_{\mathrm{LoS}_{m,j}}\, L_{\mathrm{LoS}_{m,j}} + \left(1 - p_{\mathrm{LoS}_{m,j}}\right) L_{\mathrm{NLoS}_{m,j}}, \tag{6}$$

where the LoS and NLoS path losses are expressed as

$$L_{\mathrm{LoS}_{m,j}} = 20\log_{10}\left(\frac{4\pi f d_{m,j}}{c}\right) + \xi_{\mathrm{LoS}_{m,j}}, \tag{7}$$

$$L_{\mathrm{NLoS}_{m,j}} = 20\log_{10}\left(\frac{4\pi f d_{m,j}}{c}\right) + \xi_{\mathrm{NLoS}_{m,j}}, \tag{8}$$

in which f is the carrier frequency, c is the speed of light, and $\xi_{\mathrm{LoS}_{m,j}}$ and $\xi_{\mathrm{NLoS}_{m,j}}$ are the average environment-dependent excessive path losses in dB [22]. In (6), $p_{\mathrm{LoS}_{m,j}}$ denotes the probability that UAV_m has LoS with $\mathrm{ER}_{m,j}$ [22], given by:

$$p_{\mathrm{LoS}_{m,j}} = \frac{1}{1 + a\exp\left(-b\left(\frac{180}{\pi}\theta_{m,j} - a\right)\right)}, \tag{9}$$

where a and b are constant values related to the environment, and $\theta_{m,j} = \arccos(h_{\mathrm{UAV}_m}/d_{m,j})$ is the elevation angle in radian between UAV_m and $\mathrm{ER}_{m,j}$, where $d_{m,j}$ is the Euclidean distance:

$$d_{m,j} = \sqrt{\left(x_m - x_{\mathrm{ER}_{m,j}}\right)^2 + \left(y_m - y_{\mathrm{ER}_{m,j}}\right)^2 + \left(h_m - h_{\mathrm{ER}_{m,j}}\right)^2}. \tag{10}$$

Using (6)-(10), we obtain:

$$L^{\mathrm{D}}_{\mathrm{ER}_{m,j}} = \frac{\xi_{\mathrm{LoS}_{m,j}} - \xi_{\mathrm{NLoS}_{m,j}}}{1 + a\exp\left(-b\left(\frac{180}{\pi}\theta_{m,j} - a\right)\right)} + 20\log\left(\frac{4\pi f d_{m,j}}{c}\right) + \xi_{\mathrm{NLoS}_{m,j}}. \tag{11}$$

The A2G channel model described above w.r.t. ERs (**g**) applies to the IRs (**h**) by replacing k with j and IR with ER in (5)-(11). For the G2A link $\mathrm{ER}_{m,j}$-UAV_m, the complex channel vector is denoted $\mathbf{z}_{m,j} \in \mathbb{C}^{N_\mathrm{E}\times 1}$, and we also consider a Rician model as for $\mathbf{g}_{m,j}$, with $\mathbf{z}_{m,j} = \mathbf{z}'_{m,j}/\sqrt{L^{\mathrm{U}}_{\mathrm{ER}_{m,j}}}$, and $L^{\mathrm{U}}_{\mathrm{ER}_{m,j}}$ being the average G2A distance-dependent path-loss. As for the G2G channels, the complex channel of link $\mathrm{ER}_{m,j}$-$\mathrm{IR}_{m,k}$ is denoted $e_{m,j,k}$, $m = 1,\ldots,M$, $j = 1,\ldots,J$, and $k = 1,\ldots,K$, which includes the Rayleigh fading between $\mathrm{ER}_{m,j}$ and $\mathrm{IR}_{m,k}$ as well as the path loss. Considering no LoS component as adopted in [23], $e_{m,j,k} = e'_{m,j,k}/\sqrt{L_{\mathrm{NLoS}_{m,j,k}}}$, where $e'_{m,j,k}$ is the normalized channel fading, and $L_{\mathrm{NLoS}_{m,j,k}}$ is the average path-loss similar to (8) with the distance being between $\mathrm{ER}_{m,j}$ and $\mathrm{IR}_{m,k}$.

D. Energy Transmission

For cluster m, UAV_m transmits energy signal $\mathbf{x}_{m,1} \in \mathbb{C}^{N_E\times 1}$, which consists of J energy beams, one for each ER, i.e.,

$$\mathbf{x}_{m,1} = \sqrt{\beta_m P_m}\sum_{j=1}^{J}\mathbf{w}_{m,j}\, s^{\mathrm{ER}}_{m,j}, \tag{12}$$

where P_m is the transmit power of UAV_m, $s^{\mathrm{ER}}_{m,j} \in \mathcal{CN}(0,1)$ denotes the energy-carrying signal, and $\mathbf{w}_{m,j} \in \mathbb{C}^{N_E\times 1}$ is the corresponding energy beamforming vector. Here, β_m indicates the percentage of power destined to the ERs in the m^{th} cluster, and $(1-\beta_m)$ indicates the percentage of power destined to the IRs. Hence, a larger value for β_m means that higher priority will be given to the WPT. For the j^{th} ER served by the UAV_m in the m^{th} cluster, its received signal is given by:

$$y^{\mathrm{ER}}_{m,j} = \mathbf{g}_{m,j}\sqrt{\beta_m P_m}\sum_{i=1}^{J}\mathbf{w}_{m,i}\, s^{\mathrm{ER}}_{m,i} + \sum_{l=1,l\neq m}^{M}\mathbf{g}_{l,j}\sqrt{\beta_l P_l}\sum_{i=1}^{J}\mathbf{w}_{l,i}\, s^{\mathrm{ER}}_{l,i} + n^{\mathrm{ER}}_{m,j}, \tag{13}$$

where $n^{\mathrm{ER}}_{m,j} \sim \mathcal{CN}(0,\sigma^2)$ is the AWGN, and assumed with $\sigma^2 = 1$ for all ERs. The second term in (13) represents the effect on $\mathrm{ER}_{m,j}$ from the simultaneous WPT from other UAVs to the ERs in their clusters. It is assumed that the harvested energy results from the energy signals in the cluster where the device is located, and that noise does not take part in it.[2] Assuming the availability of perfect channel state information (CSI), the optimal weight vector $\mathbf{w}^{\star}_{m,j}$ is $\mathbf{g}^{\dagger}_{m,j}/\|\mathbf{g}_{m,j}\|$. Hence, the harvested energy by $\mathrm{ER}_{m,j}$ during the first phase is given by

$$E_{m,j} = \zeta_j\alpha_m\left|\mathbf{g}_{m,j}\mathbf{w}^{\star}_{m,j}\right|^2\sum_{i=1}^{J}P^{\mathrm{D}}_{m,i} = \zeta_j\alpha_m\frac{\left\|\mathbf{g}'_{m,j}\right\|^2}{L^{\mathrm{D}}_{m,j}}P^{\mathrm{D}}_{m}, \tag{14}$$

where $0 < \zeta_j \leq 1$ is the energy-harvesting circuit efficiency [24], assumed the same for all ERs, and $P^{\mathrm{D}}_m = \beta_m P_m = \sum_{j=1}^{J}P^{\mathrm{D}}_{m,j}$ is the sum-power dedicated by UAV_m to its J ERs.

E. Information Transmission

In the second phase, ERs use the harvested energy for their uplink communication with the their associated UAV, simultaneously with the downlink transmission from the UAV to its IRs.

1) Uplink Information Transmission: The transmit power from the j^{th} ER in cluster m served by UAV_m is $P^{\mathrm{U}}_{m,j} = \frac{E_{m,j}}{1-\alpha_m}$. The UAV receives the superposed message signal of J ERs, and applies SIC to decode each device's message. The

[2]Since the energy signals that come from other clusters will be smaller compared to the signals that are beamed to the ERs in a specific cluster, we assume that their effects can be neglected.

received signal at UAV_m, is expressed as

$$\mathbf{y}_m = \sum_{j=1}^{J} \sqrt{P^{\mathrm{U}}_{m,j}}\mathbf{z}_{m,j}\, s^{\mathrm{ER}}_{m,j} + \mathbf{H}_{\mathrm{SI}_m}\sqrt{(1-\beta_m)P_m}\sum_{k=1}^{K}\mathbf{v}_{m,k}s^{\mathrm{IR}}_{m,k} + \mathbf{n}_m, \quad (15)$$

where $s^{\mathrm{ER}}_{m,j} \in \mathcal{CN}(0,1)$ is the normalized data symbol of $\mathrm{ER}_{m,j}$ towards UAV_m, $\mathbf{v}_{m,k} \in \mathbb{C}^{N_{\mathrm{I}}\times 1}$ is the corresponding beamforming vector, $s^{\mathrm{IR}}_{m,k} \in \mathcal{CN}(0,1)$ denotes the information-bearing signal of the k^{th} IR, and $\mathbf{n}_m$ is the AWGN vector with zero mean and covariance matrix $\mathbb{E}\{\mathbf{n}_m\mathbf{n}^{\dagger}_m\} = \sigma^2\mathbf{I}_{N_{\mathrm{E}}}$, where $\mathbf{I}_{N_{\mathrm{E}}}$ is the identity matrix. Further, $\mathbf{H}_{\mathrm{SI}_m} \in \mathbb{C}^{N_E\times N_I}$ is the self-interference (SI) channel due to the simultaneous uplink and downlink processes [25], with independent entries drawn from $\mathcal{CN}(0,\sigma^2_{\mathrm{SI}})$ where σ^2_{SI} account for the residual SI power after suppression [26], and it is assumed to be unity. We assume that powerful SI cancellation is in place [25], but since some SI will remain [27], we consider the effect of the residual SI.

2) Downlink Information Transmission: The data signal $\mathbf{x}_{m,2} \in \mathbb{C}^{N_I\times 1}$ sent by UAV_m to its IRs consists of K information beams, one for each IR:

$$\mathbf{x}_{m,2} = \sqrt{(1-\beta_m)P_m}\sum_{k=1}^{K}\mathbf{v}_{m,k}s^{\mathrm{IR}}_{m,k}. \quad (16)$$

In each cluster, each IR encounters interference from the uplink signals of ERs towards the UAV, as well as interference from the UAVs' downlink beams to other IRs. Hence, the received signal at $\mathrm{IR}_{m,k}$ is given by

$$y^{\mathrm{IR}}_{m,k} = \mathbf{h}_{m,k}\sqrt{(1-\beta_m)P_m}\sum_{i=1}^{K}\mathbf{v}_{m,i}s^{\mathrm{IR}}_{m,i} + \sum_{m=1}^{M}\sum_{j=1}^{J}\sqrt{P^{\mathrm{U}}_{m,j}}e_{m,j,k}s^{\mathrm{ER}}_{m,j} + \sum_{l=1,l\neq m}^{M}\mathbf{h}_{l,k}\sqrt{(1-\beta_l)P_l}\sum_{i=1}^{K}\mathbf{v}_{l,i}s^{\mathrm{IR}}_{l,i} + n^{\mathrm{IR}}_{m,k}, \quad (17)$$

where $n^{\mathrm{IR}}_{m,k} \sim \mathcal{CN}(0,\sigma^2)$ is the AWGN, and assumed with $\sigma^2 = 1$ for all IRs. In the right-hand-side of (17), the second term represents the interferences on $\mathrm{IR}_{m,k}$ from the uplink signals of ERs in all clusters, and the third term represents the interferences on $\mathrm{IR}_{m,k}$ from the downlink signals to IRs in other clusters. For any $\mathrm{IR}_{m,k}$, since the interferences from the ERs and IRs in other clusters are small compared to the interferences from ERs and other IRs in its cluster, their effects can be neglected. Assuming the availability of perfect CSI, the optimal weight vector $\mathbf{v}^{\star}_{m,k}$ is $\mathbf{h}^{\dagger}_{m,k}/\|\mathbf{h}_{m,k}\|$. Hence, the signal-to-interference-plus-noise ratio (SINR) at $\mathrm{IR}_{m,k}$ is

$$\gamma_{m,k} = \frac{Q^{\mathrm{D}}_{m,k}\left|\mathbf{h}_{m,k}\mathbf{v}^{\star}_{m,k}\right|^2}{\left(Q^{\mathrm{D}}_{m} - Q^{\mathrm{D}}_{m,k}\right)\sum_{\substack{i=1\\ i\neq k}}^{K}\left|\mathbf{h}_{m,k}\mathbf{v}^{\star}_{m,i}\right|^2 + \sum_{j=1}^{J}P^{\mathrm{U}}_{m,j}|e_{m,j,k}|^2 + 1}, \quad (18)$$

where $Q^{\mathrm{D}}_{m,k}$ is the transmit power used for the data transfer from UAV_m to $\mathrm{IR}_{m,k}$, and $Q^{\mathrm{D}}_{m} = (1-\beta_m)P_m$ is the power dedicated to the IRs.

III. Energy Efficiency Maximization

A. Energy Efficiency Formulation

To formulate the EE of the system under consideration, we have to construct the throughputs of the downlink and uplink stages for all clusters. For the downlink information NOMA setup, where the channel gains of IRs are increasing when closer to the associated UAV (channel gain of $\mathrm{IR}_{m,1}$ is larger than $\mathrm{IR}_{m,2}$, and so on until $\mathrm{IR}_{m,K}$) [28], then based on (14) and (18), the rate related to a given IR can be expressed in the unit of *bps* as shown in (19), at the bottom of the page, where W is the bandwidth, assumed the same for all GNs. According to the principles of power-domain NOMA, for a given IR, the strong interfering signals are mainly due to the transmissions towards devices with low channel gains. The weakest-channel device, $\mathrm{IR}_{m,K}$, which receives low interferences due to the relatively low powers of devices' messages with high channel gains, cannot cancel any interference. However, the device with highest channel gain, $\mathrm{IR}_{m,1}$, which receives strong interference due to the relatively high powers of the transmissions to weak devices, can cancel all interfering signals [4].

$$R^{\mathrm{D}}_{m,k} = (1-\alpha_m)\,W\log_2\left(1+\frac{\frac{Q^{\mathrm{D}}_{m,k}\left\|\mathbf{h}'_{m,k}\right\|^2}{L^{\mathrm{D}}_{\mathrm{IR}_{m,k}}(1-\alpha_m)}}{\left((1-\beta_m)P_m - Q^{\mathrm{D}}_{m,k}\right)\sum_{i=1,i\neq k}^{K}\frac{\left\|\mathbf{h}'_{m,k}\right\|^2}{L^{\mathrm{D}}_{\mathrm{IR}_{m,i}}(1-\alpha_m)} + \sum_{j=1}^{J}\frac{\zeta P^{\mathrm{D}}_{m,j}\left\|\mathbf{g}'_{m,j}\right\|^2\left\|\mathbf{z}'_{m,j}\right\|^2\left|e'_{m,j,k}\right|^2\alpha_m}{L^{\mathrm{U}}_{\mathrm{ER}_{m,j}}L^{\mathrm{D}}_{\mathrm{ER}_{m,j}}L_{\mathrm{NLoS}_{j,k}}(1-\alpha_m)} + 1}\right) \quad (19)$$

$$R^{\mathrm{U}}_{m,j} = (1-\alpha_m)\;\; W\;\; \log_2\left(1+\frac{\frac{\zeta P^{\mathrm{D}}_{m,j}\left\|\mathbf{g}'_{m,j}\right\|^2\left\|\mathbf{z}'_{m,j}\right\|^2\alpha_m}{L^{\mathrm{U}}_{\mathrm{ER}_{j,m}}L^{\mathrm{D}}_{\mathrm{ER}_{m,j}}(1-\alpha_m)}}{\left(\beta_m P_m - P^{\mathrm{D}}_{m,j}\right)\sum_{l=j+1}^{J}\frac{\zeta\left\|\mathbf{g}'_{m,l}\right\|^2\left\|\mathbf{z}'_{m,l}\right\|^2\alpha_m}{L^{\mathrm{U}}_{\mathrm{ER}_{m,l}}L^{\mathrm{D}}_{\mathrm{ER}_{m,l}}(1-\alpha_m)} + (1-\beta_m)P_m\sum_{k=1}^{K}\left\|H_{\mathrm{SI}_m}v_{m,k}\right\|^2 + 1}\right) \quad (20)$$

On the other hand, for the uplink NOMA throughput, knowing that the channel gains are stronger when ERs are closer to their UAV (channel gain of $\mathrm{ER}_{m,1}$ is larger than $\mathrm{ER}_{m,2}$, and so on until $\mathrm{ER}_{m,J}$) [28], then based on (14) and (15), the rate related to a given ER in a given cluster can be expressed as shown in (20), at the bottom of the previous page. The signal of the device with the highest channel gain, i.e., $\mathrm{ER}_{m,1}$, is decoded first at the UAV. As a result, $\mathrm{ER}_{m,1}$ experiences interference from all other ERs. Then, the signal for the second-highest channel gain device is decoded, and so on until the last device, $\mathrm{ER}_{m,J}$, [4].

For a specific UAV_m, let us define the uplink throughput as the sum-rate of all ERs in the cluster, i.e., $R_m^{\mathrm{U}} = \sum_{j=1}^{J} R_{m,j}^{\mathrm{U}}$, and the downlink throughput as the sum-rate of all IRs, i.e., $R_m^{\mathrm{D}} = \sum_{k=1}^{K} R_{m,k}^{\mathrm{D}}$. The EE of the system is expressed as

$$\eta = \frac{\sum_{m=1}^{M} (\text{Total Throughput})_m}{\sum_{m=1}^{M} (\text{Total Consumed Energy})_m} = \frac{\sum_{m=1}^{M} R_m^{\mathrm{U}} + R_m^{\mathrm{D}}}{\sum_{m=1}^{M} P_{\mathrm{DC}_m} + P_m^{\mathrm{D}} + Q_m^{\mathrm{D}}(1-\alpha_m)}, \tag{21}$$

where P_{DC_m} is the constant power consumption of UAV_m, and where $P_m^{\mathrm{D}} = \beta_m P_m = \sum_{j=1}^{J} P_{m,j}^{\mathrm{D}}$ and $Q_m^{\mathrm{D}} = (1-\beta_m)P_m = \sum_{k=1}^{K} Q_{m,k}^{\mathrm{D}}$ are the powers dedicated to the ERs and the IRs, respectively, i.e., $P_m = P_m^{\mathrm{D}} + Q_m^{\mathrm{D}}$.

B. Problem Formulation

The optimization problem which aims to maximize EE is formulated as follows:

$$\begin{aligned}
(\mathrm{OP}) \quad \max_{P_{m,j}^{\mathrm{D}}, Q_{m,k}^{\mathrm{D}}, d_{m,j}, \theta_{m,j}} \quad & \eta \\
\text{s.t.:} \quad & P_m \le P_{m,\max}, \quad \forall m, \\
& P_{m,j}^{\mathrm{U}} \le P_{m,j,\max}^{\mathrm{U}}, \quad \forall j, \forall m, \\
& \alpha_m < 1, \quad \forall m, \\
& 0 \le \beta_m \le 1, \quad \forall m, \\
& h_{m,\min} \le d_{m,j} \cos\theta_{m,j}, \ \forall j, \forall m, \\
& h_{m,\min} \le d_{m,k} \cos\theta_{m,k}, \ \forall k, \forall m, \\
& d_{m,\max} \le r_m - r_{\mathrm{UAV}_m}, \quad \forall m, \\
& \sum_{m=1}^{M} \chi_{m,j} = 1, \quad \forall j \\
& \chi_{m,j} \in \{0,1\}, \quad \forall j, \forall m \\
& \sum_{m=1}^{M} \chi_{m,k} = 1, \quad \forall k \\
& \chi_{m,k} \in \{0,1\}, \quad \forall k, \forall m \\
& R_{m,j}^{\mathrm{U}} \ge R_{m,j,\min}^{\mathrm{U}}, \quad \forall j, \forall m, \\
& R_{m,k}^{\mathrm{D}} \ge R_{m,k,\min}^{\mathrm{D}}, \quad \forall k, \forall m, \\
P_{m,\mathrm{thr}}^{\mathrm{U}} \le \ & P_{m,j}^{\mathrm{U}} z_{m,j} - \sum_{l=j+1}^{J} P_{l,j}^{\mathrm{U}} z_{l,j}, \quad \forall j, \forall m, \\
Q_{m,\mathrm{thr}}^{\mathrm{D}} \le \ & \left(Q_{m,k}^{\mathrm{D}} - \sum_{i=1, i\neq k}^{K} Q_{m,i}^{\mathrm{D}} \right) h_{m,K}, \quad \forall k, \forall m,
\end{aligned} \tag{22}$$

where $P_{m,\max}^{D}$ and $P_{m,j,\max}^{\mathrm{U}}$ are the maximum transmit powers of UAV_m and $\mathrm{ER}_{m,j}$, respectively, $h_{m,\min}$ is the minimum allowed height for UAV_m, $d_{m,\max}$ is the maximum allowable distance that UAV_m can travel during T, r_m is the cluster radius, r_{UAV_m} is the UAV radius, and where is the UAV radius, and where $R_{m,j,\min}^{\mathrm{U}}$ and $R_{m,k,\min}^{\mathrm{D}}$ denote the minimum required rates of $\mathrm{ER}_{m,j}$ and $\mathrm{IR}_{m,k}$, respectively. Finally, $P_{m,\mathrm{thr}}^{\mathrm{U}}$ and $Q_{m,\mathrm{thr}}^{\mathrm{D}}$ are the SIC detection thresholds of the uplink and downlink, $z_{m,j}$ ($\|\mathbf{z}'_{m,l}\|^2 / L_{\mathrm{ER}_{m,j}}^{\mathrm{U}}$) is the channel gain between $\mathrm{ER}_{m,k}$ and UAV_m, and $h_{m,K}$ ($\|\mathbf{h}'_{m,K}\|^2 / L_{\mathrm{IR}_{m,K}}^{\mathrm{D}}$) is the channel gain between UAV_m and $\mathrm{IR}_{m,K}$.

The optimization problem is a non-convex problem with highly coupled variables; therefore, it is hard to be solved directly by existing convex optimization methods. Accordingly, we decompose the optimization problem into two sub-problems. In the first one (OP_1), we aim to find the UAVs' optimum positions, i.e., the optimal distances and elevation angles w.r.t. the ERs and IRs according to their demands and their associations to the UAVs. After getting the UAVs' optimum positions, in the second problem (OP_2), we determine the optimal powers towards each GN in each cluster.

C. The UAV Positioning and Device Association

In OP_1, we care about $(\theta_{m,j}, d_{m,j})$ and $(\theta_{m,k}, d_{m,k})$ which are contained in (11), for all scheduled ERs and IRs that are associated with any specific UAV in each cluster at the same time. This can be achieved by connecting the path losses for A2G channels related to each GN by the parameters pertaining to the nodes' demands. So, OP_1 will be as follows:

$$\begin{aligned}
(\mathrm{OP}_1) \quad \min_{d_{m,j}, d_{m,k}, \theta_{m,j}, \theta_{m,k}} \quad & \sum_j \Upsilon_j^{\mathrm{U}} L_{\mathrm{ER}_{m,j}}^{\mathrm{D}} + \sum_k \Upsilon_k^{\mathrm{D}} L_{\mathrm{IR}_{m,k}}^{\mathrm{D}} \\
\text{s.t.:} \quad & h_{m,\min} \le d_{m,j} \cos\theta_{m,j}, \ \forall j, \forall m, \\
& h_{m,\min} \le d_{m,k} \cos\theta_{m,k}, \ \forall k, \forall m, \\
& d_{m,\max} \le r_m - r_{\mathrm{UAV}_m}, \ \forall m, \\
& \sum_{m=1}^{M} \chi_{m,j} = 1, \quad \forall j \\
& \chi_{m,j} \in \{0,1\} \quad \forall j, \forall m \\
& \sum_{m=1}^{M} \chi_{m,k} = 1, \quad \forall k \\
& \chi_{m,k} \in \{0,1\} \quad \forall k, \forall m.
\end{aligned} \tag{23}$$

As mentioned, at the beginning of the process, each UAV will be hovering at the minimum allowable height over the center of its cluster, and each device (ERs or IRs) to be served will send its ID to the UAV of its cluster. Accordingly, $\chi_{m,j}$ of each ER and $\chi_{m,k}$ of each IR that ask to be served in each cluster can be determined. This optimization problem can be solved by introducing the Lagrangian multipliers $\mathbf{\Omega_{IR}}_m \ge 0$ and $\mathbf{\Omega_{ER}}_m \ge 0$, where $\mathbf{\Omega_{IR}}_m = [\Omega_{\mathrm{IR}_{m,1}}, \Omega_{\mathrm{IR}_{m,2}}, \ldots, \Omega_{\mathrm{IR}_{m,K}}]$ and $\mathbf{\Omega_{ER}}_m = [\Omega_{\mathrm{ER}_{m,1}}, \Omega_{\mathrm{ER}_{m,2}}, \ldots, \Omega_{\mathrm{ER}_{m,J}}]$. The objective function then becomes

$$\mathcal{L}_1\left(\mathbf{\Omega_{ER}}_m, \mathbf{\Omega_{IR}}_m, \boldsymbol{d_{m,j}}, \boldsymbol{d_{m,k}}, \boldsymbol{\theta_{m,j}}, \boldsymbol{\theta_{m,k}}\right)$$

$$= \sum_{j=1}^{J} \Upsilon_j^{\mathrm{U}} L_{\mathrm{ER_{m,j}}}^{\mathrm{D}} + \sum_{k=1}^{K} \Upsilon_k^{\mathrm{D}} L_{\mathrm{IR}_{m,k}}^{\mathrm{D}} - \sum_{j=1}^{J} \Omega_{\mathrm{ER}_{m,j}} \big(h_{m,\min} - d_{m,j} \cos\theta_{m,j}\big) - \sum_{k=1}^{K} \Omega_{\mathrm{IR}_{m,k}} \big(h_{m,\min} - d_{m,k} \cos\theta_{m,k}\big). \quad (24)$$

Exploiting the Karush-Kuhn-Tucker (KKT) conditions, one can obtain the optimal position of the UAV by solving the first derivatives of $\mathcal{L}_1$ w.r.t. $d_{m,j}$, $d_{m,k}$, $\theta_{m,j}$ and $\theta_{m,k}$, respectively, as follows:

$$\frac{\partial \mathcal{L}_1}{\partial d_{m,j}} = \Upsilon_j^{\mathrm{U}} \frac{\partial L_{\mathrm{ER}_{m,j}}^{\mathrm{D}}}{\partial d_{m,j}} - \Omega_{\mathrm{ER}_{m,j}} \cos\theta_{m,j} = \frac{20\Upsilon_j^{\mathrm{U}}}{d_{m,j}\ln(10)} - \Omega_{\mathrm{ER}_{m,j}} \cos\theta_{m,j} = 0, \quad (25)$$

$$\frac{\partial \mathcal{L}_1}{\partial d_{m,k}} = \Upsilon_k^{\mathrm{D}} \frac{\partial L_{\mathrm{IR}_{m,k}}^{\mathrm{D}}}{\partial d_{m,k}} - \Omega_{\mathrm{IR}_{m,k}} \cos\theta_{m,k} = \frac{20\Upsilon_k^{\mathrm{D}}}{d_{m,k}\ln(10)} - \Omega_{\mathrm{IR}_{m,k}} \cos\theta_{m,k} = 0, \quad (26)$$

$$\frac{\partial \mathcal{L}_1}{\partial \theta_{m,j}} = \Upsilon_j^{\mathrm{U}} \frac{\partial L_{\mathrm{ER}_{m,j}}^{\mathrm{D}}}{\partial d_{m,j}} + \Omega_{\mathrm{ER}_{m,j}} d_{m,j} \cos\theta_{m,j} = \frac{\Upsilon_j^{\mathrm{U}}\, ab \frac{180}{\pi} (\xi_{\mathrm{LoS}} - \xi_{\mathrm{NLoS}}) \exp\big(-b\big(\frac{180}{\pi}\theta_{m,j} - a\big)\big)}{\big(1 + a\exp\big(-b\big(\frac{180}{\pi}\theta_{m,j} - a\big)\big)\big)^2} + \Omega_{\mathrm{ER}_{m,j}} d_{m,j} \cos\theta_{m,j} = 0, \quad (27)$$

$$\frac{\partial \mathcal{L}_1}{\partial \theta_{m,k}} = \Upsilon_k^{\mathrm{D}} \frac{\partial L_{\mathrm{IR}_{m,k}}^{\mathrm{D}}}{\partial d_{m,k}} + \Omega_{\mathrm{IR}_{m,k}} d_{m,k} \cos\theta_{m,k} = \frac{\Upsilon_k^{\mathrm{D}}\, ab \frac{180}{\pi} (\xi_{\mathrm{LoS}} - \xi_{\mathrm{NLoS}}) \exp\big(-b\big(\frac{180}{\pi}\theta_{m,k} - a\big)\big)}{\big(1 + a\exp\big(-b\big(\frac{180}{\pi}\theta_{m,k} - a\big)\big)\big)^2} + \Omega_{\mathrm{IR}_{m,k}} d_{m,k} \cos\theta_{m,k} = 0. \quad (28)$$

The new values of $\Omega_{\mathrm{ER}_{m,j}}$ and $\Omega_{\mathrm{IR}_{m,k}}$ can be calculated using the gradient-descent method [29]:

$$\Omega_{\mathrm{ER}_{m,j}}(i+1) = \Big[\Omega_{\mathrm{ER}_{m,j}}(i) - \Delta_{\Omega_{\mathrm{ER}_{m,j}}} \big(h_{m,\min} - d_{m,j}\cos\theta_{m,j}\big)\Big]^{+}, \quad (29)$$

$$\Omega_{\mathrm{IR}_{m,k}}(i+1) = \Big[\Omega_{\mathrm{IR}_{m,k}}(i) - \Delta_{\Omega_{\mathrm{IR}_{m,k}}} \big(h_{m,\min} - d_{m,k}\cos\theta_{m,j}\big)\Big]^{+}, \quad (30)$$

where $\Omega_{\mathrm{ER}_{m,j}}(i)$ and $\Omega_{\mathrm{IR}_{m,k}}(i)$ are respectively the values of $\Omega_{\mathrm{IR}_{m,k}}$ and $\Omega_{\mathrm{ER}_{m,j}}$ at the i^{th} iteration, $\Delta_{\Omega_{\mathrm{ER}_{m,j}}}$ and $\Delta_{\Omega_{\mathrm{IR}_{m,k}}}$ are the iteration steps. The output of the optimization will be the optimum positions of the UAVs. Algorithm 1 summarizes the procedure. The results will be used in the second optimization problem.

Algorithm 1 3D UAV Location Optimization

Input: Υ_j^{U}, Υ_k^{D}, ξ_{LoS}, ξ_{NLoS} a, b, $h_{m,\min}$, f, r_m, $r_{\mathrm{UAV_m}}$, and GNs' ID, $\forall j$, $\forall k$, $\forall m$.

Output: $(x_m, y_m, h_m)^*$, $\forall m$.

Initialization: $(x_m, y_m, h_m)^0$, $\Omega_{\mathrm{ER}_{m,j}} = 0$, $\Omega_{\mathrm{IR}_{m,k}} = 0$, $\forall j$, $\forall k$, $\forall m$.

1: Determine $\chi_{m,j}$, as per (1) and (3), $\forall j$, $\forall m$.
2: Determine $\chi_{m,k}$, as per (2) and (4), $\forall k$, $\forall m$.
3: Update $\Omega_{\mathrm{ER}_{m,j}}$ and $\Omega_{\mathrm{IR}_{m,k}}$ according to (29) and (30).
4: Solve (25) for $d_{m,j}$, $\forall j$, $\forall m$.
5: Solve (26) for $d_{m,k}$, $\forall k$, $\forall m$.
6: Solve (27) for $\theta_{m,j}$, $\forall j$, $\forall m$.
7: Solve (28) for $\theta_{m,k}$, $\forall k$, $\forall m$.
8: Compute the optimal $(x_m, y_m, h_m)^*$, $\forall m$, by solving (23).

D. Energy-Efficient Resource Allocation

Based on the constraints that have been treated in OP_1, and the results of Algorithm 1, we formulate OP_2 as follows:

$$\begin{aligned}(\mathrm{OP}_2) \quad \max_{P_{m,j}^{\mathrm{D}}, Q_{m,k}^{\mathrm{D}}} \quad & \eta \\ \text{s.t.:} \quad & P_m \le P_{m,\max}, \quad \forall m, \\ & P_{m,j}^{\mathrm{U}} \le P_{m,j,\max}^{\mathrm{U}}, \quad \forall j, \forall m, \\ & \alpha_m < 1, \quad \forall m, \\ & 0 \le \beta_m \le 1, \quad \forall m, \\ & R_{m,j}^{\mathrm{U}} \ge R_{m,j,\min}^{\mathrm{U}}, \quad \forall j, \forall m, \\ & R_{m,k}^{\mathrm{D}} \ge R_{m,k,\min}^{\mathrm{D}}, \quad \forall k, \forall m, \\ & P_{m,\mathrm{thr}}^{\mathrm{U}} \le P_{m,j}^{\mathrm{U}} z_{m,j} - \sum_{l=j+1}^{J} P_{m,l}^{\mathrm{U}} z_{m,l}, \\ & \forall j, \forall m, \\ & Q_{m,\mathrm{thr}}^{\mathrm{D}} \le \left(Q_{m,k}^{\mathrm{D}} - \sum_{i=1, i\neq k}^{K} Q_{m,i}^{\mathrm{D}}\right) h_{m,K}, \\ & \forall k, \forall m. \end{aligned} \quad (31)$$

It is obvious that OP_2 is a fractional optimization problem with the variables $P_{m,j}^{\mathrm{D}}$ and $Q_{m,k}^{\mathrm{D}}$, and is non-convex. Exploiting the idea in [30], the fractional programming problem can be transformed into a convex problem by introducing the variable F^* as the optimal EE when we have the optimal power for each ER and IR. Accordingly, the objective function becomes $\sum_{m=1}^{M} R_m^{\mathrm{U}} + R_m^{\mathrm{D}} - F^* \sum_{m=1}^{M} (P_{\mathrm{DC}_m} + P_m^{\mathrm{D}} + Q_m^{\mathrm{D}}(1 - \alpha_m))$. By introducing $\boldsymbol{\vartheta} \ge 0$, $\boldsymbol{\varsigma_m} \ge 0$, $\boldsymbol{\varepsilon} \ge 0$, $\boldsymbol{\varrho} \ge 0$, $\boldsymbol{\varphi_m} \ge 0$, $\boldsymbol{\lambda_m} \ge 0$, $\boldsymbol{\mu_m} \ge 0$, and $\boldsymbol{\rho_m} \ge 0$, as the Lagrange multipliers associated with the constraints in OP_2, where $\boldsymbol{\vartheta} = [\vartheta_1, \vartheta_2, \ldots, \vartheta_M]$, $\boldsymbol{\varsigma_m} = [\varsigma_{m,1}, \varsigma_{m,2}, \ldots, \varsigma_{m,J}]$, $\boldsymbol{\varepsilon} = [\varepsilon_1, \varepsilon_2, \ldots, \varepsilon_M]$, $\boldsymbol{\varrho} = [\varrho_1, \varrho_2, \ldots, \varrho_M]$, $\boldsymbol{\varphi_m} = [\varphi_{m,1}, \varphi_{m,2}, \ldots, \varphi_{m,J}]$, $\boldsymbol{\lambda_m} = [\lambda_{m,1}, \lambda_{m,2}, \ldots, \lambda_{m,K}]$, $\boldsymbol{\mu_m} = [\mu_{m,1}, \mu_{m,1}, \ldots, \mu_{m,J}]$, and $\boldsymbol{\rho_m} = [\rho_{m,1}, \rho_{m,1}, \ldots, \rho_{m,K}]$, then the Lagrangian function of OP_2 can be formulated as:

$$\mathcal{L}_2(\boldsymbol{\vartheta}, \boldsymbol{\varsigma_m}, \boldsymbol{\varepsilon}, \boldsymbol{\varrho}, \boldsymbol{\varphi_m}, \boldsymbol{\lambda_m}, \boldsymbol{\mu_m}, \boldsymbol{\rho_m}, Q_{m,k}^{\mathrm{D}}, P_{m,j}^{\mathrm{D}})$$

$$= \sum_{m=1}^{M} R_m^{\mathrm{U}} + R_m^{\mathrm{D}} - F^* \sum_{m=1}^{M} \left(P_{\mathrm{DC}_m} + P_m^{\mathrm{D}} + Q_m^{\mathrm{D}}(1-\alpha_m)\right) - \sum_{m=1}^{M} \vartheta_m (P_m - P_{m,\max}) - \sum_{m=1}^{M}\sum_{j=1}^{J} \varsigma_{m,j}\left(P_{m,j}^{\mathrm{U}} - P_{m,j,\max}^{\mathrm{U}}\right) - \sum_{m=1}^{M} \varepsilon_m(\alpha_m - 1) - \sum_{m=1}^{M}\sum_{j=1}^{J} \varphi_{m,j}\left(R_{m,j,\min}^{\mathrm{U}} - R_{m,j}^{\mathrm{U}}\right) - \sum_{m=1}^{M} \varrho_m(\beta_m - 1) - \sum_{m=1}^{M}\sum_{k=1}^{K} \lambda_{m,k}\left(R_{m,k,\min}^{\mathrm{D}} - R_{m,k}^{\mathrm{D}}\right) - \sum_{m=1}^{M}\sum_{j=1}^{J} \mu_{m,j}\left[P_{m,\mathrm{thr}}^{\mathrm{U}} - P_{m,j}^{\mathrm{U}} z_{m,j} - \sum_{l=j+1}^{J} P_{m,l}^{\mathrm{U}} z_{m,l}\right] - \sum_{m=1}^{M}\sum_{k=1}^{K} \rho_{m,k}\left[Q_{m,\mathrm{thr}}^{\mathrm{D}} - \left(Q_{m,k}^{\mathrm{D}} - \sum_{i=1,i\neq k}^{K} Q_{m,i}^{\mathrm{D}}\right) h_{m,K}\right]. \quad (32)$$

Our goal is to find the optimized $Q_{m,k}^{\mathrm{D}}$ and $P_{m,j}^{\mathrm{D}}$. We assume that UAV_m uses its maximum power, such that $\beta_m P_{m,\max} = P_m^{\mathrm{D}}$ and $(1-\beta_m)P_{m,\max} = Q_m^{\mathrm{D}}$. Taking into account that OP_2 is a nonlinear programming problem, this can be done through derivation of the Lagrangian function (32) w.r.t. $Q_{m,k}^{\mathrm{D}}$ and $P_{m,j}^{\mathrm{D}}$, and then setting them to zero, i.e.,

$$\frac{\partial \mathcal{L}_2\left(\boldsymbol{\vartheta}, \boldsymbol{\varsigma_m}, \boldsymbol{\varepsilon}, \boldsymbol{\varrho}, \boldsymbol{\varphi_m}, \boldsymbol{\lambda_m}, \boldsymbol{\mu_m}, \boldsymbol{\rho_m}, Q_{m,k}^{\mathrm{D}}, P_{m,j}^{\mathrm{D}}\right)}{\partial Q_{m,k}^{\mathrm{D}}} = 0, \quad (33)$$

$$\frac{\partial \mathcal{L}_2\left(\boldsymbol{\vartheta}, \boldsymbol{\varsigma_m}, \boldsymbol{\varepsilon}, \boldsymbol{\varrho}, \boldsymbol{\varphi_m}, \boldsymbol{\lambda_m}, \boldsymbol{\mu_m}, \boldsymbol{\rho_m}, Q_{m,k}^{\mathrm{D}}, P_{m,j}^{\mathrm{D}}\right)}{\partial P_{m,j}^{\mathrm{D}}} = 0. \quad (34)$$

The updating of the Lagrangian variables ($\boldsymbol{\vartheta}$, $\boldsymbol{\varsigma_m}$, $\boldsymbol{\varepsilon}$, $\boldsymbol{\varrho}$, $\boldsymbol{\varphi_m}$, $\boldsymbol{\lambda_m}$, $\boldsymbol{\mu_m}$, and $\boldsymbol{\rho_m}$) can be done using the gradient-descent method:

$$\vartheta_m(i+1) = \left[\vartheta_m(i) - \Delta_{\vartheta_m}(P_{m,\max} - P_m)\right]^+, \quad (35)$$

$$\varsigma_{m,j}(i+1) = \left[\varsigma_{m,j}(i) - \Delta_{\varsigma_{m,j}}\left(P_{m,j,\max}^{\mathrm{U}} - P_{m,j}^{\mathrm{U}}\right)\right]^+, \quad (36)$$

$$\varepsilon_m(i+1) = \left[\varepsilon_m(i) - \Delta_{\varepsilon_m}(1-\alpha_m)\right]^+, \quad (37)$$

$$\varrho_m(i+1) = \left[\varrho_m(i) - \Delta_{\varrho_m}(1-\beta_m)\right]^+, \quad (38)$$

$$\varphi_{m,j}(i+1) = \left[\varphi_{m,j}(i) - \Delta_{\varphi_{m,j}}\left(R_{m,j,\min}^{\mathrm{U}} - R_{m,j}^{\mathrm{U}}\right)\right]^+, \quad (39)$$

$$\lambda_{m,k}(i+1) = \left[\lambda_{m,k}(i) - \Delta_{\lambda_{m,k}}\left(R_{m,k,\min}^{\mathrm{D}} - R_{m,k}^{\mathrm{D}}\right)\right]^+, \quad (40)$$

$$\mu_{m,j}(i+1) = \left[\mu_{m,j}(i) - \Delta_{\mu_{m,j}}\left(P_{m,\mathrm{thr}}^{\mathrm{U}} - P_{m,j}^{\mathrm{U}} z_{m,j} - \sum_{l=j+1}^{J} P_{m,l}^{\mathrm{U}} z_{m,l}\right)\right]^+, \quad (41)$$

$$\phi_{m,k}(i+1) = \left[\phi_{m,k}(i) - \Delta_{\phi_{m,k}}\left(Q_{m,\mathrm{thr}}^{\mathrm{D}} - \left(Q_{m,k}^{\mathrm{D}} - \sum_{i=1,i\neq k}^{K} Q_{m,i}^{\mathrm{D}}\right) h_{m,K}\right)\right]^+, \quad (42)$$

Algorithm 2 Energy-Efficient Resource Allocation

Input: $(x_m, y_m, h_m)^*$, ξ_{LoS}, ξ_{NLoS}, a, b, $h_{m,\min}$, GNs' ID, f, η, σ, $R_{\min}^{\mathrm{D}}$ and $R_{\min}^{\mathrm{U}}$, $\forall j$, $\forall k$, $\forall m$.
Output: $(Q_{m,k}^{\mathrm{D}}, P_{m,j}^{\mathrm{D}})^*$.
Initialization: $(Q_{m,k}^{\mathrm{D}}, P_{m,j}^{\mathrm{D}})^0$, $\boldsymbol{\vartheta} = \mathbf{0}$, $\boldsymbol{\varsigma}_m = \mathbf{0}$, $\boldsymbol{\varepsilon} = \mathbf{0}$, $\boldsymbol{\varrho} = \mathbf{0}$ $\boldsymbol{\varphi}_m = \mathbf{0}$, $\boldsymbol{\lambda}_m = \mathbf{0}$, $\boldsymbol{\mu}_m = \mathbf{0}$, $\boldsymbol{\rho}_m = \mathbf{0}$.
1: Update the Lagrangian variables, $\boldsymbol{\vartheta}$, $\boldsymbol{\varepsilon}$, $\boldsymbol{\varrho}$, $\boldsymbol{\lambda_m}$, and $\boldsymbol{\rho_m}$ based on (35), (37), (38), (40), and (42), respectively.
2: Solve (33) for $Q_{m,k}^{\mathrm{D}}$.
3: Update the Lagrangian variables, $\boldsymbol{\vartheta}$, $\boldsymbol{\varsigma_m}$, $\boldsymbol{\varepsilon}$, $\boldsymbol{\varrho}$, $\boldsymbol{\varphi_m}$, and $\boldsymbol{\mu_m}$ based on (35), (36), (37), (38), (39), and (41), respectively.
4: Solve (34) for $P_{m,j}^{\mathrm{D}}$.
5: Compute $(Q_{m,k}^{\mathrm{D}}, P_{m,j}^{\mathrm{D}})^*$, $\forall m$, $\forall k$, $\forall j$, by solving (31).

where i is the iteration index, and the Δ's are the iteration steps.

The solution of OP_2 is summarized in Algorithm 2.

E. Complexity Analysis

In the previous section, we explained that the optimization problem under consideration is a highly coupled non-convex problem, thus it is extremely difficult to be solved. However, with the suggested sub-optimal approach, we decomposed the problem into two sub-problems and were able to solve them efficiently by with the proposed algorithms. Both algorithms are based on the gradient-descent method, where the worst complexity of such method is $\boldsymbol{O}(n \times \frac{1}{\epsilon})$ [31], with n being the number of optimization variables and ϵ the solution accuracy. Thus, for Algorithm 1, the complexity depends on the 3D plane size that the UAVs consider for moving, i.e., $x \times y \times (h_{m,\max} - h_{m,\min})$, where $(h_{m,\max} - h_{m,\min})$ is the allowable altitude range for moving. For Algorithm 2, the complexity depends on the numbers of UAVs (M), ERs (J), and IRs (K). As such, the total complexity of the algorithms is $\boldsymbol{O}(x \times y \times (h_{m,\max} - h_{m,\min}) \times \frac{1}{\epsilon}) + \boldsymbol{O}(M \times (J+K) \times \frac{1}{\epsilon})$.

IV. Numerical Results

In this section, taking into account the details of the system and channel models explained in Section II, we evaluate the proposed algorithms' effectiveness in single- and multiple-UAV scenarios. In the special case of single-UAV system, we show the details of the scheduled GNs and the effect of each of them on the overall performance. This also reflects the situation in any given cluster in the multiple-UAV scenario. The main simulation parameters are shown in Table I. We adopt UAV parameters to meet the specifications of existing small UAVs that can handle this kind of UAV-based communications [32], and assume urban propagation environment [22], unless stated otherwise.

A. Single-UAV Scenario

In this scenario, which means there is only one cluster for the ROI (100×100 m^2), we consider that the center of the region is (0, 0). For the GNs' distribution, we consider that

TABLE I
MAIN SIMULATION PARAMETERS

Parameter	Notation	Value
Operating Frequency	f	2 GHz
Average excessive path loss (LoS)	ξ_{LoS}	1 dB
Average excessive path loss (NLoS)	ξ_{NLoS}	20 dB
Energy-harvesting circuit efficiency	η	0.8
Number of antennas at the UAV	N	4
Constant power consumption of the UAV	P_{DC}	5 Watt
Maximum transmit power of the UAV	$P_{\max}$	3 Watt
Uplink SIC detection threshold	$P^{\text{U}}_{\text{thr}}$	0.05 Watt
Downlink SIC detection threshold	$Q^{\text{D}}_{\text{thr}}$	0.05 Watt
ER's minimum required rate	$R^{\text{U}}_{\min}$	12 Kbps
IR's minimum required rate	$R^{\text{D}}_{\min}$	12 Kbps
Channel parameters for the urban environment	a, b	9.6, 0.28

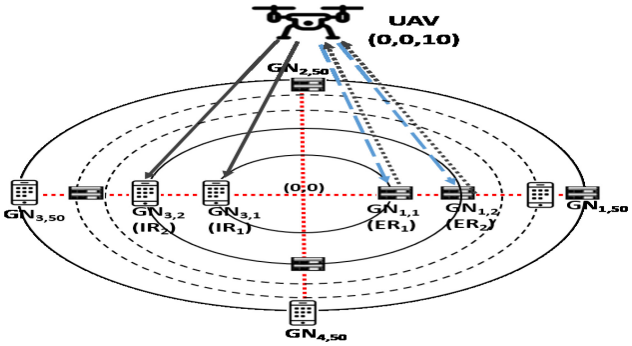

Fig. 3. Single-UAV scenario.

the circles are uniformly formulated by increasing 1 m for the radius from the center, with the segments formed by increasing the angle of a segment by $\pi/2$ from the positive horizontal plane, i.e., $\phi = 1, \ldots, 50$, $\psi = 1, \ldots, 4$. Fig. 3 illustrates the single-UAV scenario. We consider four GNs requesting service at the same time; two are ERs, and two are IRs. Nodes $\text{GN}_{1,1}$, i.e., ER_1, and $\text{GN}_{3,1}$, i.e., IR_1, have fixed positions and always ask to be served. The other two devices, ER_2 and IR_2, are $\text{GN}_{1,2}$ and $\text{GN}_{3,2}$, in the simulations, we vary their positions horizontally on both sides of the cluster center, ER_2 in the side of ER_1 and IR_2 in the side of IR_1. Note that ER_1 and IR_1 are always closer to the cluster center. All GNs have the same rate demands, i.e., $\Upsilon^{\text{U}}_1 = \Upsilon^{\text{U}}_2 = \Upsilon^{\text{D}}_1 = \Upsilon^{\text{D}}_2 = 0.25$. The UAV hovers at the minimum allowable height over the cluster center, i.e., (0, 0, 10).

As a first stage of the process, β is determined before starting the actual transmissions towards the devices. According to the symmetrical positions of ERs and IRs in our setup, the power budget is split equally between the energy and data transmissions. Once β is obtained, the transmissions towards the ERs and IRs start. Fig. 4 shows the throughput of each of the two IRs along with the summation of those rates. It is clear that the throughput of IR_1 always outperforms that of IR_2 for both the OMA and NOMA schemes. For NOMA, throughput is constructed according to (19). With the OMA protocol, the UAV sends the information separately by dedicating half of the transmission phase, $(1-\alpha)/2$, to each IR. The sum-rate with OMA is better than with NOMA for small distances of IR_2 w.r.t. the UAV, while NOMA starts to outperform OMA as the said distance increases, where the link of IR_2 becomes much weaker compared to the link of the strong GN. Energy harvested by the ERs from the downlink WPT is used for their NOMA uplink communication with the UAV.

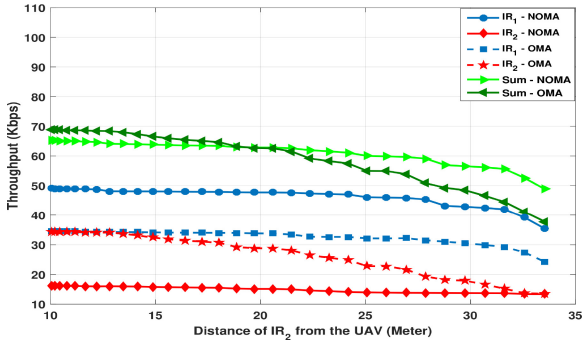

Fig. 4. Downlink throughput in single-UAV scenario.

Figure 5 illustrates the throughput of each ER along with the sum-rate. Results of conventional uplink OMA, where each ER sends its information to the UAV during half of the second phase, i.e., $(1-\alpha)/2$, are also provided. It is obvious that the throughput of ER_1 mostly outperforms the one of ER_2 in the OMA set-up. With NOMA, there are some variations and correlations between the rates of ER_1 and ER_2. As observed, the throughput of ER_1 decreases sharply when ER_2 is closer to the UAV, which implicitly means that its transmission increases the interference on the signal of ER_1. This can be clearly noticed when the distance of ER_2 is less than 13 m, which means that it starts to have a strong connection with the UAV. In the OMA and NOMA schemes, the rate of ER_1 starts to decrease when the distance of ER_2 from the UAV increases, which is due to the minimum rate constraints in both schemes. As the rate of ER_2 must also satisfy the said constraints, and with decreasing channel gain with the distance, this is compensated by dedicating more power towards ER_2 on the account of ER_1, in both OMA and NOMA. It is clear that the NOMA-based uplink's sum-rate is larger than the OMA's due to the simultaneous transmissions from the ERs.

Figure 6 compares the effect of the access schemes on the system's EE. Results are plotted as a function of the distance of ER_2 from the UAV, taking into account that the downlink throughput of IR_2 is constructed from the same distance of the uplink throughput of ER_2. The EE with the NOMA scheme is considerably better than that with OMA for different distances of ER_2 w.r.t. the UAV, and the difference increases as the distance of ER_2 from the UAV increases. It is important to note that when the said distance is small and that the ERs and IRs are close to each other, the difference in the performance between OMA and NOMA is tight due to the loss of the required distinctions between users in NOMA. However, the interferences from the ERs to the IRs have more effect on the OMA-based scenario as compared to NOMA.

B. Multiple-UAV Scenario

Now, we consider that there are 4 UAVs ($M = 4$) to cover the ROI of 100x100 m^2, which also means that we have four clusters, each with a radius of 25 m. The centers of clusters 1, 2, 3 and 4 are (25, 25), (75, 25), (75, 75) and (25, 75), respectively. For the GNs' distribution, we consider that the circles are formed by increasing 1 m the radius from the center of each cluster, with the segments formed by increasing the angle of a segment by $\pi/2$ from the positive horizontal plane

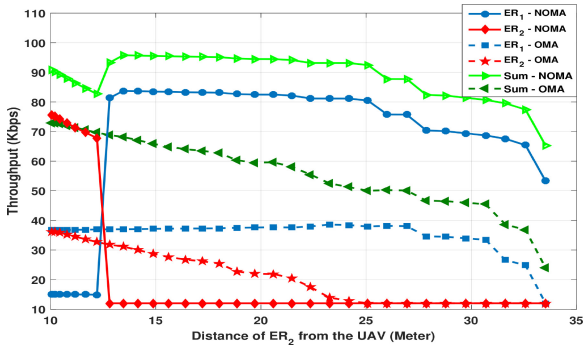

Fig. 5. Uplink throughput in the single-UAV scenario.

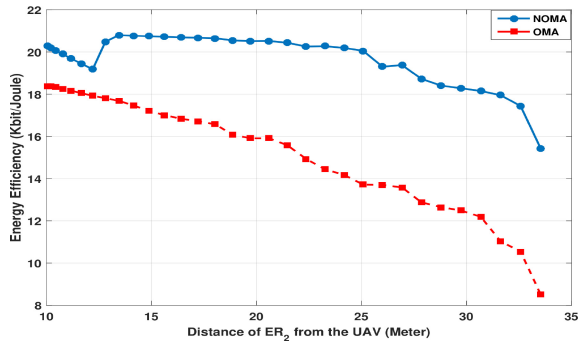

Fig. 6. Energy efficiency in the single-UAV scenario.

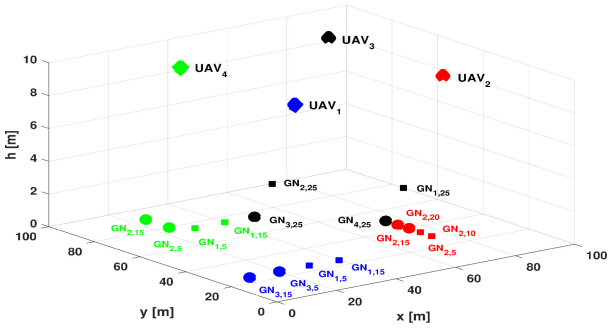

Fig. 7. The locations of the UAVs in Case-1.

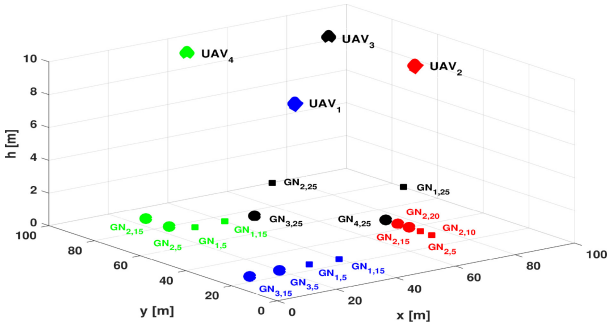

Fig. 8. The optimal locations of the UAVs in Case-2.

in each cluster, i.e., $\phi = 1, \ldots, 25$, $\psi = 1, \ldots, 4$, in each cluster. For the simulations, we consider that 16 GNs ask to be served at the same time, 4 in each cluster. In cluster 1, $\mathrm{GN}_{1,5}$ and $\mathrm{GN}_{1,15}$ are ERs, and $\mathrm{GN}_{3,5}$ and $\mathrm{GN}_{3,15}$ are IRs. In cluster 2, $\mathrm{GN}_{2,5}$ and $\mathrm{GN}_{2,10}$ are ERs, and $\mathrm{GN}_{2,15}$ and $\mathrm{GN}_{2,20}$ are IRs. In cluster 3, $\mathrm{GN}_{1,25}$ and $\mathrm{GN}_{2,25}$ are ERs, and $\mathrm{GN}_{3,25}$ and $\mathrm{GN}_{4,25}$ are IRs. In cluster 4, $\mathrm{GN}_{1,5}$ and $\mathrm{GN}_{1,15}$ are ERs, and $\mathrm{GN}_{2,5}$ and $\mathrm{GN}_{2,15}$ are IRs. In this multiple-UAV scenario, we consider four different cases according to different combinations of the GNs' demands.

- Case-1 "No consideration for the GNs' service demands": Each UAV will hover at the minimum allowable height over the center of its cluster.
- Case-2 "Equal service demands for all GNs in a cluster" (e.g., in any cluster, $\Upsilon_1^{\mathrm{U}} = \Upsilon_2^{\mathrm{U}} = \Upsilon_1^{\mathrm{D}} = \Upsilon_2^{\mathrm{D}} = 0.25$): At the beginning of the process, each UAV hovers at the minimum allowable height over the center of its cluster, and then moves to the optimal position according to the GNs' service demands.
- Case-3 "Different service demand for each GN in a cluster, $\Upsilon^{\mathrm{U}} > \Upsilon^{\mathrm{D}}$": The service demands for ERs are higher than those of IRs (e.g., in any cluster, $\Upsilon_1^{\mathrm{U}} + \Upsilon_2^{\mathrm{U}} = 0.75$, and $\Upsilon_1^{\mathrm{D}} + \Upsilon_2^{\mathrm{D}} = 0.25$). First, each UAV hovers at the minimum allowable height over the center of its cluster, and then moves to the optimal position according to these different GNs' service demands.
- Case-4 "Different service demand for each GN in a cluster, $\Upsilon^{\mathrm{D}} > \Upsilon^{\mathrm{U}}$": The service demands of IRs are higher than the ones of ERs (e.g., in any cluster, $\Upsilon_1^{\mathrm{U}} + \Upsilon_2^{\mathrm{U}} = 0.25$, and $\Upsilon_1^{\mathrm{D}} + \Upsilon_2^{\mathrm{D}} = 0.75$). Each UAV initially hovers at the minimum allowable height over the center of its cluster, and then moves to the optimal position according to the GNs' service demands.

1) 3D Positions of the UAVs: As the GNs' service demands will not be taken into account in Case-1, the four UAVs will be hovering at the minimum allowable height over the centers of their clusters. These positions will be fixed in the whole process. As shown in Fig. 7, the positions are (25, 25, 10) for UAV_1, (75, 25, 10) for UAV_2, (75, 75, 10) for UAV_3, and (25, 75, 10) for UAV_4, For the remaining cases (2, 3 and 4), the UAVs will move from the initial positions to the optimal points according to Algorithm 1. In Case-2, this will be depending on the same service demands of all GNs in each cluster; hence, the optimal positions of UAV_1, UAV_2, UAV_3 and UAV_4 will be (25, 25, 10), (75, 37.5, 10), (75, 75, 10) and (35,85,10), respectively, as shown in Fig. 8. We note that each UAV will relocate its position to be somewhere between all scheduled GNs in its cluster, as the demands are the same for all of them.

In Case-3, where the demands of ERs are higher than the ones of IRs, each UAV will take the optimal position to be near the ERs to be able to meet their demands. Thus, the optimal positions of UAV_1, UAV_2, UAV_3, and UAV_4 will be (35, 25, 10), (75, 32.5, 10), (87.5, 87.5, 10) and (35, 75, 10), respectively, as shown in respectively, as shown in Fig. 9.

When the service demands of IRs are greater as compared to the ones of the ERs as defined in Case-4, the UAV in each cluster moves towards the IRs to satisfy their demands. Fig. 10 shows the optimal positions of the UAVs in the ROI. The positions are (15, 25, 10) for UAV_1, (75, 42.5, 10) for UAV_2, UAV_2, (62.5, 62.5, 10) for UAV_3, and (25, 85, 10) for UAV_4.

Figure 11 shows the 2D optimal positions of the UAVs for the four cases. This explains the changes of the positions of

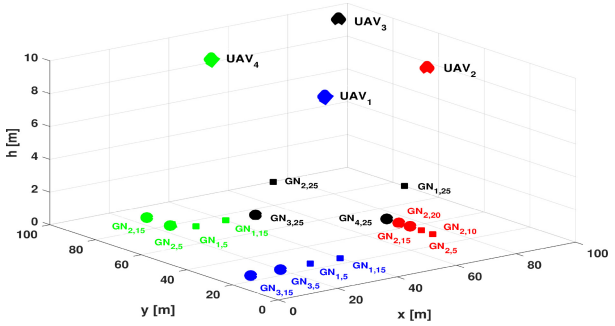

Fig. 9. The optimal locations of the UAVs in Case-3.

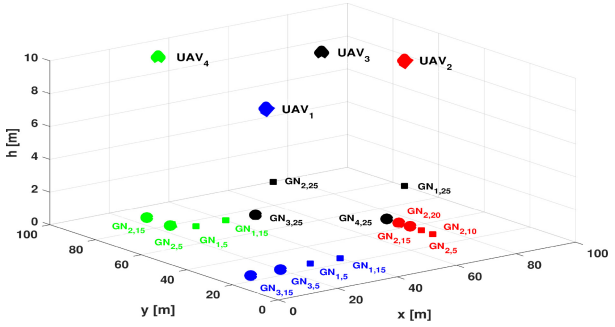

Fig. 10. The optimal locations of the UAVs in Case-4.

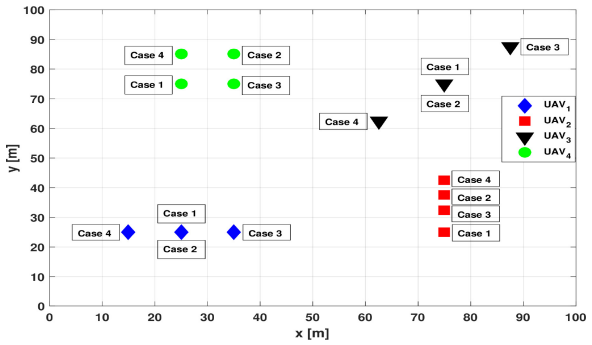

Fig. 11. The 2D optimal locations of the UAVs in the four cases.

the UAVs from one case to another. Note that the height is fixed for all UAVs in all cases.

2) EE Optimization: We compare the performance resulting from applying the algorithms to the four cases for NOMA and OMA schemes as shown in Fig. 12, which illustrates the EE w.r.t. the normalized charging time (α) which is set the same for all UAVs. One can notice that NOMA outperforms OMA in all cases. Also, the difference between the NOMA based cases are more considerable than those of the OMA based cases. However, the differences vary from case to case. It is clear that the EE for Case-2, which considers equal service demands for all GNs, is the best compared to the other cases for NOMA and OMA schemes. Compared to Case-1, which does not consider the GNs' service demands at all, we notice that the UAVs' positioning in Case-2 enhances the system EE, as all UAVs provide better links for all GNs in their clusters. However, the EE in Case-1 outperforms those in cases 3 and 4, where the GNs' demands are also considered, and this also shows the effect of the distribution of the scheduled nodes on the overall performance. For Case-3, where the demands

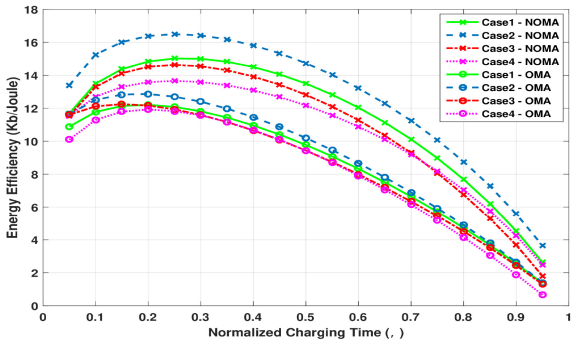

Fig. 12. System energy efficiency versus normalized charging time.

of ERs are more significant than the ones of IRs, the UAVs move closer to the ERs, providing them with much stronger links compared to the IRs. This degrades the total downlink throughput for IRs, which is reflected in the system EE. For Case-4, where the demands of IRs are more extensive than the ones of ERs, the UAVs travel towards the IRs to meet their needs. This severely degrades the total uplink throughput of ERs, as they depend on the links for receiving the power on the downlink and then use it on the uplink, so both links are affected and this is reflected in the EE.

V. Conclusion

In this work, we investigated the resource allocation in a network deploying multiple multi-antenna UAVs for transmitting data to IRs and energy to ERs to enable their uplink data communication. A general highly coupled non-convex optimization problem was formulated to maximize the network's EE while satisfying many constraints related to the user association, UAVs positions, power budgets, collision avoidance, acceptable QoS, and SIC thresholds. The problem was solved after decomposing it into two sub-problems by minimizing the path losses of the A2G channels according to the devices' demands, and then optimizing the transmit powers towards maximization of the EE. The results showed the superiority of the system operation with NOMA verus OMA. Notably, for the single-UAV case, it was shown that EE of the NOMA-based network outperforms that of OMA in most cases w.r.t. the position of the weak user. Also, for different multiple-UAV scenarios, the EE with NOMA was shown to be better than that with OMA, where the case with equal rate requirements has the best performance.

References

[1] S. Najmeddin, S. Aïssa, and S. Tahar, "Energy-efficient resource allocation for UAV-enabled information and power transfer with NOMA," in *Proc. IEEE Global Commun. Conf.*, 2020, pp. 1–6.

[2] Z. Xue, J. Wang, G. Ding, and Q. Wu, "Joint 3D location and power optimization for UAV-enabled relaying systems," *IEEE Access*, vol. 6, pp. 43113–43124, 2018.

[3] X. Zhou, R. Zhang, and C. K. Ho, "Wireless information and power transfer: Architecture design and rate-energy tradeoff," in *Proc. IEEE Global Commun. Conf.*, 2012, pp. 3982–3987.

[4] M. S. Ali, H. Tabassum, and E. Hossain, "Dynamic user clustering and power allocation for uplink and downlink non-orthogonal multiple access (NOMA) systems," *IEEE Access*, vol. 4, pp. 6325–6343, 2016.

[5] S. M. R. Islam, N. Avazov, O. A. Dobre, and K.-S. Kwak, "Power-domain non-orthogonal multiple access (NOMA) in 5G systems: Potentials and challenges," *IEEE Commun. Surveys Tuts.*, vol. 19, no. 2, pp. 721–742, 2nd Quart., 2017.

[6] M. F. Sohail, C. Y. Leow, and S. Won, "Non-orthogonal multiple access for unmanned aerial vehicle assisted communication," *IEEE Access*, vol. 6, pp. 22716–22727, 2018.
[7] L. Xie, J. Xu, and R. Zhang, "Throughput maximization for UAV-enabled wireless powered communication networks," *IEEE Internet Things J.*, vol. 6, no. 2, pp. 1690–1703, Apr. 2019.
[8] S. Najmeddin, A. Bayat, S. Aïssa, and S. Tahar, "Energy-efficient resource allocation for UAV-enabled wireless powered communications," in *Proc. IEEE Wireless Commun. Netw. Conf.*, 2019, pp. 1–6.
[9] M. Alzenad, A. El-Keyi, F. Lagum, and H. Yanikomeroglu, "3-D placement of an unmanned aerial vehicle base station (UAV-BS) for energy-efficient maximal coverage," *IEEE Wireless Commun. Lett.*, vol. 6, no. 4, pp. 434–437, Aug. 2017.
[10] H. He, S. Zhang, Y. Zeng, and R. Zhang, "Joint altitude and beamwidth optimization for UAV-enabled multiuser communications," *IEEE Commun. Lett.*, vol. 22, no. 2, pp. 344–347, Feb. 2018.
[11] Z. Wang, L. Duan, and R. Zhang, "Adaptive deployment for UAV-aided communication networks," *IEEE Trans. Wireless Commun.*, vol. 18, no. 9, pp. 4531–4543, Sep. 2019.
[12] S. Yin, Y. Zhao, and L. Li, "UAV-assisted cooperative communications with time-sharing SWIPT," in *Proc. IEEE Int. Conf. Commun.*, May 2018, pp. 1–6.
[13] C. Jeong and S. H. Chae, "Simultaneous wireless information and power transfer for multi-user UAV-enabled IoT networks," *IEEE Internet Things J.*, vol. 8, no. 10, pp. 8044–8055, May 2021.
[14] F. Huang *et al.*, "UAV-assisted SWIPT in Internet of Things with power splitting: Trajectory design and power allocation," *IEEE Access*, vol. 7, pp. 68260–68270, 2019.
[15] W. Mei and R. Zhang, "Uplink cooperative NOMA for cellular-connected UAV," *IEEE J. Sel. Topics Signal Process.*, vol. 13, no. 3, pp. 644–656, Jun. 2019.
[16] S. Jeong, O. Simeone, and J. Kang, "Mobile edge computing via a UAV-mounted cloudlet: Optimization of bit allocation and path planning," *IEEE Trans. Veh. Technol.*, vol. 67, no. 3, pp. 2049–2063, Mar. 2018.
[17] V. V. Chetlur and H. S. Dhillon, "Downlink coverage analysis for a finite 3-D wireless network of unmanned aerial vehicles," *IEEE Trans. Commun.*, vol. 65, no. 10, pp. 4543–4558, Oct. 2017.
[18] S. Enayati, H. Saeedi, H. Pishro-Nik, and H. Yanikomeroglu, "Moving aerial base station networks: A stochastic geometry analysis and design perspective," *IEEE Trans. Wireless Commun.*, vol. 18, no. 6, pp. 2977–2988, Jun. 2019.
[19] F. Huang, J. Chen, H. Wang, G. Ding, Y. Gong, and Y. Yang, "Multiple-UAV-assisted SWIPT in Internet of Things: User association and power allocation," *IEEE Access*, vol. 7, pp. 124244–124255, 2019.
[20] Y. Zeng, Q. Wu, and R. Zhang, "Accessing from the sky: A tutorial on UAV communications for 5G and beyond," *Proc. IEEE*, vol. 107, no. 12, pp. 2327–2375, Dec. 2019.
[21] D. Romero and G. Leus, "Non-cooperative aerial base station placement via stochastic optimization," in *Proc. Int. Conf. Mobile Ad-Hoc Sens. Netw.*, 2019, pp. 131–136.
[22] A. Al-Hourani, S. Kandeepan, and S. Lardner, "Optimal LAP altitude for maximum coverage," *IEEE Wireless Commun. Lett.*, vol. 3, no. 6, pp. 569–572, Dec. 2014.
[23] M. Mohammadi, B. K. Chalise, H. A. Suraweera, and Z. Ding, "Wireless information and power transfer in full-duplex systems with massive antenna arrays," in *Proc. IEEE Int. Conf. Commun.*, 2017, pp. 1–6.
[24] M. Xia and S. Aissa, "On the efficiency of far-field wireless power transfer," *IEEE Trans. Signal Process.*, vol. 63, no. 11, pp. 2835–2847, Jun. 2015.
[25] T. Riihonen, S. Werner, and R. Wichman, "Mitigation of loopback self-interference in full-duplex MIMO relays," *IEEE Trans. Signal Process.*, vol. 59, no. 12, pp. 5983–5993, Dec. 2011.
[26] H. Q. Ngo, H. A. Suraweera, M. Matthaiou, and E. G. Larsson, "Multipair full-duplex relaying with massive arrays and linear processing," *IEEE J. Sel. Areas Commun.*, vol. 32, no. 9, pp. 1721–1737, Sep. 2014.
[27] Y. He, H. Zhao, W. Guo, S. Shao, and Y. Tang, "A time-robust digital self-interference cancellation in full-duplex radios: Receiver design and performance analysis," *IEEE Access*, vol. 8, pp. 185021–185031, 2020.
[28] T. A. Zewde and M. C. Gursoy, "NOMA-based energy-efficient wireless powered communications," *IEEE Trans. Green Commun. Netw.*, vol. 2, no. 3, pp. 679–692, Sep. 2018.
[29] S. Boyd and L. Vandenberghe, *Convex Optimization*. Cambridge, U.K.: Cambridge Univ. Press, 2004.
[30] D. W. K. Ng, E. S. Lo, and R. Schober, "Energy-efficient resource allocation for secure OFDMA systems," *IEEE Trans. Veh. Technol.*, vol. 61, no. 6, pp. 2572–2585, Jul. 2012.
[31] Y. Nesterov, *Lectures on Convex Optimization*. Cham, Switzerland: Springer, 2018.
[32] C. Yan, L. Fu, J. Zhang, and J. Wang, "A comprehensive survey on UAV communication channel modeling," *IEEE Access*, vol. 7, pp. 107769–107792, 2019.

Saif Najmeddin (Graduate Student Member, IEEE) received the B.Sc. degree in communication and electronic engineering from Palestine Polytechnic University (PPU), Al-Khalil, Palestine, in 2011, and the M.Sc. degree in communication engineering from King Fahd University of Petroleum and Minerals, Dhahran, Saudi Arabia, in 2015. He is currently pursuing the Ph.D. degree with Concordia University and Institut National de la Recherche Scientifique, Montreal, QC, Canada.

From 2011 to 2012, he was a full-time Network Engineer with Royal Company and a part-time Research Assistant with PPU. His current research interests include wireless communication, communication networks, and UAV-assisted communications.

Sonia Aïssa (Fellow, IEEE) received the Ph.D. degree in electrical and computer engineering from McGill University, Montreal, QC, Canada, in 1998.

Since then, she has been with the Institut National de la Recherche Scientifique (INRS), Montreal, where she is a Full Professor. From 1996 to 1997, she was a Researcher with the Department of Electronics and Communications, Kyoto University, Japan, and with the Wireless Systems Laboratories, NTT, Japan. From 1998 to 2000, she was a Research Associate with INRS. From 2000 to 2002, while she was an Assistant Professor, she was a Principal Investigator in the major program of personal and mobile communications with the Canadian Institute for Telecommunications Research, leading research in radio resource management for wireless networks. From 2004 to 2007, she was an Adjunct Professor with Concordia University, Canada. She was a Visiting Invited Professor with Kyoto University, in 2006, and with Universiti Sains Malaysia, in 2015. Her research interests include the modeling, design and performance analysis of wireless communication systems and networks, and wireless power.

Prof. Aïssa awards include the NSERC University Faculty Award in 1999; the Quebec Government FRQNT Strategic Faculty Fellowship in 2001–2006; the INRS Performance Award multiple times since 2004, for outstanding achievements in research, teaching and outreach; and the 2007 Technical Community Service Award from the FRQNT Centre for Advanced Systems and Technologies in Communications. She is recipient of multiple IEEE Best Paper Awards and of the 2012 IEICE Best Paper Award; and recipient of NSERC Discovery Accelerator Supplement Award. She is the Founding Chair of the IEEE Women-In-Engineering Montreal, from 2004 to 2007; served as the TPC Symposium Chair or Co-Chair at IEEE ICC '06 '09 '11 '12; the Program Co-Chair at IEEE WCNC 2007; the TPC Co-Chair of IEEE VTC-S 2013; the TPC Symposia Chair of IEEE Globecom 2014; the TPC Vice-Chair of IEEE Globecom 2018; and the TPC Chair of IEEE ICC 2021. Her editorial activities include: the Editor-at-Large of IEEE TRANSACTIONS ON COMMUNICATIONS since 2020; an Area Editor of IEEE TRANSACTIONS ON WIRELESS COMMUNICATIONS, from 2014 to 2019; an Editor of IEEE TRANSACTIONS ON WIRELESS COMMUNICATIONS, from 2004 to 2012; an Associate Editor and the Technical Editor of *IEEE Communications Magazine*, from 2004 to 2015; the Technical Editor of *IEEE Wireless Communications Magazine*, from 2006 to 2010; and an Associate Editor of *Security and Communication Networks* (Wiley) from 2007 to 2012. She served as a Distinguished Lecturer of the IEEE Communications Society and a Member of its Board of Governors from 2013 to 2016 and from 2014 to 2016. She is a Fellow of the Canadian Academy of Engineering.

Sofiène Tahar (Senior Member, IEEE) received the Diploma degree in computer engineering from the University of Darmstadt, Germany, in 1990, and the Ph.D. degree (Hons.) in computer science from the University of Karlsruhe, Germany, in 1994. He is currently a Professor and the Research Chair of Formal Verification of Systems-on-Chip with the Department of Electrical and Computer Engineering, Concordia University, Montreal, QC, Canada, where he is also the Founder and the Director of the Hardware Verification Group. His research interests include formal hardware verification, system-on-chip verification, AMS circuit verification, and probabilistic, statistical, and reliability analysis.